JOURNAL OF CLIMATE

Indian summer monsoon rainfall interannual variability: spatial signatures and teleconnections

SPENCER A. HILL *

Lamont-Doherty Earth Observatory, Columbia University, Palisades, New York

ADAM H. SOBEL

Department of Applied Physics and Applied Mathematics and Lamont-Doherty Earth Observatory, Columbia University, New York, New York

MICHELA BIASUTTI, MARK A. CANE

Lamont-Doherty Earth Observatory, Columbia University, Palisades, New York

ABSTRACT

A widely used indicator of Indian summer monsoon variability is the June-July-August-September (JJAS) rainfall rate averaged over all of India (AIR). But AIR's relationship with the spatial extent of dry or wet anomalies across India is contested, its relationship with El Niño-Southern Oscillation (ENSO) has weakened since the early 20th century, and its relationship with the Equatorial Indian Ocean Oscillation (EQUINOO) has only been examined for the late 20th and 21st centuries. We explore these issues using long-duration (1901-2020), sea surface temperature, reanalysis, and high-resolution rainfall ($0.25^\circ \times 0.25^\circ$) gridded rainfall datasets. AIR is highly correlated ($r > 0.95$) both with indices determined predominantly by raw rainfall anomalies in the high-variance Central Monsoon Zone and Western Ghats regions and with indices we define characterizing the spatial extent of standardized rainfall anomalies across all of India: the high-rainfall regions dictate AIR *and* vary closely with the extent of drought or excess rainfall over the subcontinent. The JJAS rainfall regression patterns for ENSO and EQUINOO change in compensating ways from the pre-satellite to satellite eras, such that a combined index, ENSINOO, is more stable and corresponds to widespread drying or wetting. Because EQUINOO exhibits strong variance on daily as well as seasonal timescales, however, it is not obvious to what extent its seasonal-mean signal reflects a remotely forced teleconnection vs. the residual of larger, shorter-timescale variability.

1. Introduction

Indian summer monsoon rainfall varies on temporal scales from hourly to decadal and spatial scales from a few meters to the whole country. This rich spectrum of variability in Earth's strongest monsoon circulation (e.g. Nie et al. 2010) profoundly influences the lives of India's more than billion citizens and Earth's general circulation. As such, accurate predictions of Indian summer monsoon rainfall variability have been sought since at least the 19th century (e.g. reviews by Gadgil 2003, 2018). Prediction efforts often focus on arguably the simplest bulk measure of the summer monsoon, the all-India rainfall average, or AIR, averaged over the summer monsoon season of June-July-August-September (JJAS). Societally, JJAS AIR is well correlated with interannual deviations in Indian agricultural yields and gross domestic product (Gadgil and Gadgil 2006). Physically, it is intuitive and a direct measure of the total diabatic heating generated over the subcontinent by the summer monsoon (though importantly this neglects the rainfall over neighboring countries and oceanic points).

Because AIR is an integral measure of local rainfall rates across India, its interannual variability will be most influenced by those parts of the country where the local rainfall interannual variability is high. Monsoonal India includes two such regions, as can be seen in Fig. 1 showing the climatological JJAS rainfall of monsoonal India (from a gridded $0.25^\circ \times 0.25^\circ$ dataset to be detailed later). To first order the interannual variance scales with the mean, with the largest values of both (exceeding 36 mm day^{-1} for the mean and 10 mm day^{-1} for the standard deviation in some gridpoints) occurring within the narrow coastal band between the Arabian Sea coast and the Western Ghats (WG) mountains. These sharp gradients in the southwest have dictated the border definitions of subdivisions of the In-

*Corresponding author address: Spencer Hill, 207B Oceanography, Lamont-Doherty Earth Observatory, 61 Route 9W, Palisades, NY 10964
E-mail: shill@ldeo.columbia.edu

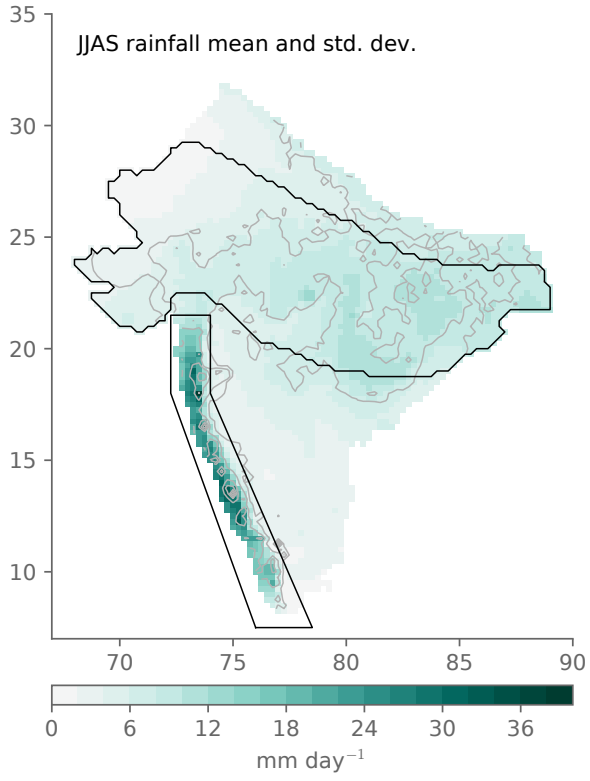

FIG. 1. Climatological JJAS rainfall mean in colors and standard deviation in grey contours in the IMD 0.25×0.25° gridded dataset, 1901-2020, both with units mm day^{-1} and with contour interval 2 mm day^{-1}.

dian Meteorological Department station network since the 19th century (Blanford 1886; Gadgil et al. 1993; Kelkar and Sreejith 2020) but are likely unresolved in gridded datasets with resolutions of 1° or more. Values are also high over a broad swath of northern-central India, which, c.f. Gadgil et al. (2019), we refer to as the Central Monsoon Zone (CMZ). Values are lower in Southeast India, where the rainy season occurs during the "northeast" monsoon in boreal autumn rather than in JJAS.

Given this spatial heterogeneity, in principle AIR need not be a useful indicator of the spatial extent of wet or dry anomalies: an average spanning regions with high variance and regions with low variance will depend primarily on the former and weakly on the latter — even if relative to the local mean (i.e. the coefficient of variation) and/or standard deviation (i.e. standardized anomalies) the anomalies in the low-variance region are large. Subseasonally, this is precisely what occurs in the so-called active-break cycle operating on a roughly weekly timescale: in active periods, rainfall is enhanced over the WG and CMZ, rainfall is suppressed in peninsular India between the WG and CMZ, and AIR is high; in break periods, anomalies are the opposite sign (e.g. Rajeevan et al. 2010). This overall spatial pattern of large-magnitude, same-signed loadings spanning the CMZ and WG, with weak and/or opposite-signed loadings in peninsular India sandwiched between, emerges in numerous subseasonal contexts such as: daily snapshots of satellite cloud cover imagery (Sikka and Gadgil 1980); composites based on the presence of monsoon low pressure systems (Krishnamurthy and Ajayamohan 2010); cluster analysis of ∼monthly rainfall variability (Moron et al. 2017); composites on the phase of the Madden-Julian Oscillation (Pai et al. 2011); composites based on intraseasonal active/break phases of monsoon rainfall (Krishnamurthy and Shukla 2007, 2008; Rajeevan et al. 2010); and the first empirical orthogonal function (EOF) computed from daily JJAS rainfall standardized anomalies (Krishnamurthy and Shukla 2000).

However, variability of daily rainfall on quasi-weekly timescales need not operate in the same manner as seasonal-mean rainfall on interannual timescales. In their influential series of studies, Krishnamurthy and Shukla (2000, 2007, 2008) argue that the primary seasonally persisting mode of JJAS AIR variability is distinct from the active-break signal and brings quasi-homogeneous drying or wetting throughout India. Such a signal is often associated with the teleconnection from the El Niño-Southern Oscillation (ENSO), with drying more likely during El Niño and wetting more likely during La Niña events (e.g. Rasmusson and Carpenter 1983). But correlations of AIR with various ENSO indices have always left the majority of AIR variance unexplained (e.g. Surendran et al. 2015) and have weakened in recent decades compared to the early 20th century (e.g. Ashok et al. 2019).

It is also the case that, except for some extreme years to be discussed below, JJAS-mean rainfall anomalies are quite heterogeneous across different regions of India, which requires mechanisms beyond quasi-uniform wetting or drying. Given that for JJAS rainfall daily variance exceeds seasonal-mean variance by an order of magnitude over most of India (Krishnamurthy and Shukla 2000), this could well reflect the seasonal residual of shorter timescale variability (Charney and Shukla 1981; Palmer 1994). But Krishnamurthy and Shukla (2008) use advanced spectral techniques (multi-channel singular spectrum analysis) to identify an additional seasonally-persisting mode of JJAS-mean variability distinct both from the quasi-uniform seasonal mode and the residual of subseasonal variability. And the OLR pattern spanning the broader Indo-West Pacific region associated with this mode resembles another seasonal-timescale teleconnection mode, the Equatorial Indian Ocean Oscillation (EQUINOO) [compare bottom panels of Fig. 7 and Fig. 8b of Krishnamurthy and Shukla (2008) with e.g. Fig. 1 of Francis and Gadgil (2013)]. EQUINOO can be thought of as the atmospheric counterpart to the Indian Ocean Dipole (IOD) oceanic oscillatory mode spanning the equatorial Indian ocean (Saji

et al. 1999; Webster et al. 1999), albeit with weaker atmosphere-ocean coupling between EQUINOO and the IOD compared to ENSO (Gadgil et al. 2003, 2004). In EQUINOO's positive phase, convection is enhanced in the western equatorial Indian Ocean (and over the subcontinent) relative to the eastern equatorial Indian Ocean (Gadgil et al. 2003, 2004).

What are the interrelationships among ENSO, EQUINOO, and the subseasonal variability just discussed? For the period 1958-2010, Surendran et al. (2015) find ENSO and EQUINOO essentially uncorrelated, and therefore a linear combination of ENSO and EQUINOO they introduce is significantly better correlated with AIR at lag-zero than either mode is alone. But to our knowledge, the behavior of EQUINOO in the early 20th century has not been investigated, in particular whether, like ENSO, its relationship with Indian summer monsoon rainfall has changed.

Motivated by newly available long-duration, high-resolution datasets of Indian rainfall, reanalyzed winds, and sea surface temperatures, the present study revisits the spatial heterogeneity of summer-mean rainfall variability in monsoonal India using 120-year observed or reanalyzed timeseries, 1901-2020, of all relevant fields. We also deliberately restrict to methods that are minimally statistically involved, opting for simplicity of interpretation at the likely expense of some insights afforded by more advanced techniques. Those data and methods are detailed in Section 2. We then argue that both interpretations of AIR — controlled by high-variance regions vs. reflecting the extent of drying across all of India including lower-variance regions — are essentially true: AIR is predominantly controlled by rainfall in the CMZ and WG regions, but the magnitude and sign of the rainfall anomalies in these regions tracks very closely with the overall spatial extent of drying or wetting throughout the subcontinent (Section 3). For teleconnections, we find that the EQUINOO rainfall regression over India resembles the subseasonal active-break phase composite, which combined with pronounced daily-timescale variability of the EQUINOO index muddies its interpretation as a remotely forced teleconnection (Section 4). Nevertheless, we then show that the well-known decrease in the correlation of AIR with ENSO going from the pre-satellite to satellite eras is largely countered by an increase in the correlation of AIR with EQUINOO, such that a combined ENSO-EQUINOO index is highly correlated with AIR over both epochs (Section 5). Finally, we conclude with summary and discussion (Section 6).

2. Methods

a. Rainfall

We use the Indian Meteorological Department (IMD) daily, gridded $0.25\times0.25^\circ$ rainfall dataset spanning 1901-2020 (Pai et al. 2014). Daily values from 1 June to 30 September are averaged, forming a JJAS seasonal-mean for each year. To focus on monsoon-related rainfall, we apply the mask of Gadgil et al. (2019) that excludes northern India, where the vicinity to the Himalayas and extratropical influences make interannual rainfall variability not clearly related to the monsoonal circulation. Another reason for excluding Northeast India is that there appear to be spurious data points in a cluster of grid cells on the border of Bangladesh, with the JJAS mean and variance jumping in 1971 to implausible values over the remainder of the record (not shown). The mean JJAS rainfall restricting to monsoonal India is very highly correlated with the all-India rainfall average computed without the monsoon mask, $r = 0.95$ (not shown). And many other past studies exclude points in far north and northeast India as well (e.g. Krishnamurthy and Shukla 2000; Vecchi and Harrison 2004). Therefore for simplicity henceforth we will refer to the monsoonal-India average as AIR.

We also compute averages over the CMZ and WG regions, whose borders are shown as black contours in Fig. 1 and subsequent map panels. The CMZ boundaries follow Gadgil et al. (2019). We define the WG borders to align with the sharp rainfall gradient separating the coastal and inland peninsular regimes. In terms of IMD meteorological subdivisions, the WG region roughly corresponds to, but extends further inland than, the union of three existing subdivisions, Konkan and Goa, Coastal Karnataka, and Kerala (e.g. Kelkar and Sreejith 2020). The CMZ and WG surface areas are 52.1 and 9.3% respectively of the monsoonal India surface area, and climatologically they harbor 52.8 and 19.8% of the rain that falls in monsoonal India in JJAS. The remaining 38.6% of monsoonal India therefore receives 27.4% of all-India rainfall climatologically.

We have compared the IMD dataset with the TRMM 3B42v7 (Huffman et al. 2007) daily dataset over the period 1998-2014. While on any given day the differences calculated from the two datasets over India can be substantial (not shown), the JJAS AIR timeseries between the two datasets are very highly correlated ($r = 0.94$). For all fields analyzed, 1901-2020 trends (computed by simple least squares regression) are modest compared to their interannual standard deviations (not shown). Nevertheless for all analyses we subtract of this linear trend to focus on interannual variability. At scales exceeding a few gridpoints results are qualitatively insensitive to this methodological choice (not shown). All correlations and regressions are performed at zero lag.

b. Teleconnections

For ENSO, we use the NINO3.4 index computed from the Extended Reconstruction SST (ERSST; Huang et al. 2015) monthly observational dataset, 1901-2020. This is almost perfectly correlated ($r = 0.99$) with NINO3.4

computed from the NOAA Optimal Interpolation OI SST dataset (Reynolds et al. 2002) over 1982-2019. The correlations of AIR with NINO3.4 vs. NINO3 are nearly identical ($r = -0.53$) and moderately lower in magnitude for NINO4 ($r = -0.40$). The rainfall regression and correlation patterns also look very similar for each of the three NINO indexes (not shown). We therefore focus on NINO3.4 from ERSST exclusively henceforth for ENSO.

For EQUINOO, we use the "equatorial wind" or EQWIN index, defined as the near-surface zonal wind anomaly averaged over the central equatorial Indian Ocean, 60-90°E, 2.5°S-2.5°N (Francis and Gadgil 2013). For 1901-1949, monthly, ensemble-mean winds are taken from the CERA-20C reanalysis dataset (Laloyaux et al. 2018), an ensemble-based, extended reanalysis dataset that only assimilates surface observations and spans 1901-2010. For 1950-2020, hourly winds from the new ERA5 reanalysis (Hersbach et al. 2020) are averaged into daily and JJAS means. We combine these two timeseries into a single EQWIN index spanning 1901-2020, by first concatenating the two timeseries (i.e. CERA-20C for 1901-1949 and ERA5 for 1950-2020; note that 1950-1978 uses the provisional "extended" portion of the ERA5 dataset), detrending, and finally normalizing by the standard deviation. EQWIN computed in the CERA-20C and ERA5 datasets is highly correlated during their overlapping span of 1951-2010 ($r = 0.87$), which we take as justification for the use of the combined timeseries. As done for the IMD rainfall data, we subtract off the linear trend over the 120 year period of all teleconnection mode indices.

We have compared EQWIN to an alternative index of EQUINOO based on outgoing longwave radiation (OLR), EQUINOLR (Francis and Gadgil 2013), defined as the difference in outgoing longwave radiation (OLR) averaged over boxes in the eastern and western equatorial Indian Ocean (90-110°E, 10°S-0° and 50-70°E, 10°S-10°N, respectively. JJAS-averaged EQWIN and EQUINOLR are correlated at $r = 0.68$ in CERA-20C and $r = 0.76$ in ERA5 over each dataset's full range, and all major EQUINOO-related results discussed are qualitatively insensitive to which index is used (not shown).

3. Relationships between all-India and sub-India rainfall variations

a. Sub-India regions of coherent rainfall variability and their inter-relationships

Fig. 2 shows the fraction of annual-mean rainfall that occurs in JJAS. Over most of the WG and CMZ that fraction exceeds 80%, in parts of the far west more than 95%, in stark contrast to values below one-third in the far southeast. Overlain surface elevation contours illustrate how orography organizes JJAS-mean rainfall variability within peninsular India. Southwesterly low-level summer monsoon flow acting on the sharp elevation gradient generates

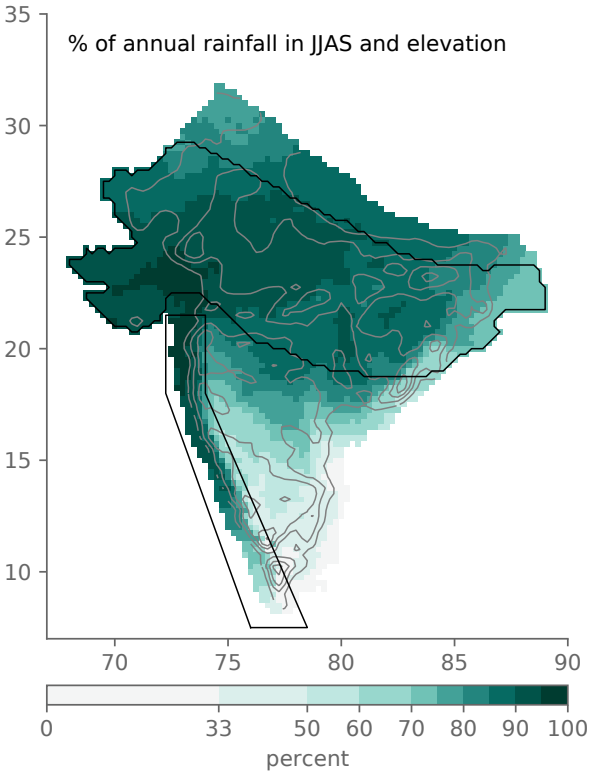

FIG. 2. In color shading, climatological fraction of annual-mean rainfall that occurs during JJAS in color shading. In grey contours, surface elevation in 200 m increments starting at 200 m.

a narrow, high-rainfall coastal band on the windward side and a broader, drier regime on the leeward side over the Deccan Plateau (e.g. Francis and Gadgil 2006; Hunt et al. 2021).

Fig. 3 shows the correlation between JJAS-mean rainfall at each gridpoint with that at each of three selected gridpoints, one each in the CMZ, WG, and peninsular India between CMZ and WG (c.f. Gadgil et al. 1993; Vecchi and Harrison 2004). From these pointwise correlation maps (and those of other points not shown), three distinct regions emerge: CMZ, WG, which appear correlated with each other, and southeast India, whose variability is independent or modestly anti-correlated with that of CMZ and WG.

Fig. 4(a) shows the AIR, CMZ, and WG region-mean anomaly timeseries, and Fig. 5(a) shows a cross-correlation matrix of these timeseries as well as others to be described later. AIR is well correlated with WG ($r = 0.78$) and even more so with CMZ ($r = 0.93$). The CMZ and WG anomalies are themselves appreciably correlated ($r = 0.59$). And AIR is very highly correlated with a linear combination of the CMZ and WG averages ($r = 0.96$) with weights 84% and 16%, respectively ap-

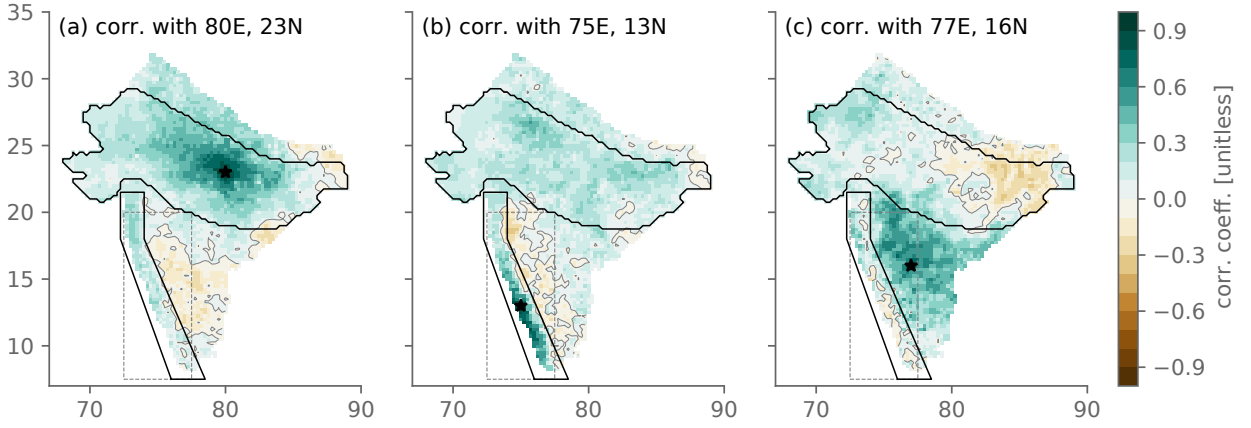

FIG. 3. Correlation of JJAS rainfall at each gridpoint with that of the gridpoint labeled and indicated by the black star. Solid black curves denote the borders of the Western Ghats (along the Arabian Sea coast) and Central Monsoon Zone (spanning northern India) regions. The dashed, gray rectangles indicate the extent of the WG region borders used by Vecchi and Harrison (2004).

plied to the raw regional averages. These weights were chosen to maximize the correlation with AIR; it happens that the $16/84 \approx 0.19$ ratio of the WG to CMZ weights approximately equals that of the WG and CMZ surface areas (expressed as fractions of the total monsoonal India area, $9.3\%/52.1\% \approx 0.18$).

We compute two alternative all-India indices that emphasize the spatial extent of rainfall anomalies rather than their raw integral; both are included in Fig. 4(c) and Fig. 5(a). The first is the standardized rainfall anomaly averaged over all gridpoints of monsoonal India, rather than the raw rainfall anomaly as in AIR. It is almost perfectly correlated with AIR ($r = 0.98$) and very highly correlated with the CMZ-WG linear combination ($r = 0.91$). The second is simply for each year the number of gridpoints in which the local JJAS rainfall anomaly is positive. It too is very highly correlated with AIR ($r = 0.96$) and the CMZ-WG linear combination ($r = 0.89$). As such, there is no contradiction between interpreting AIR as primarily reflecting the high-variance sub-regions of India vs. as reflecting the extent of local drying or wetting across all of India: the former interpretation is true almost by construction, and the latter happens to be true as well.

b. Empirical orthogonal functions

Another way of showing these connections of AIR to rainfall in the CMZ and WG on the one hand and to the spatial extent of drying/wetting on the other hand is through EOF analysis. Fig. 6(a) shows the first EOF of seasonal-mean JJAS rainfall anomalies computed from each gridpoint's raw rainfall anomaly, which accounts for 18.9% of the total variance. The EOF pattern resembles the mean and interannual standard deviation with values highest within WG, also elevated over most of the CMZ, and smallest in peninsular India between WG and CMZ. This resemblance is quantified in Fig. 5(b), a pattern correlation matrix that includes these fields and others to be discussed. The mean, standard deviation, and EOF spatial patterns are well correlated with one another ($r = 0.74$-0.83). And the corresponding principal component (PC) timeseries (shown in Fig. 4b and included in the correlation matrix in Fig. 5a) is very highly correlated with the AIR timeseries ($r = 0.95$).

Fig. 6(b) shows the EOF computed from standardized rather than raw rainfall anomalies (c.f. Krishnamurthy and Shukla 2000), which accounts for 18.2% of the JJAS-mean rainfall total variance. Relative to the EOF computed from raw rainfall anomalies, the pattern is more homogeneous, with loadings decreased over much of WG and increased in the far west, northwest, much of the CMZ, and much of peninsular India. As such, the pattern correlations with the mean and standard deviation fields are slightly negative ($r = -0.18$ and $r = -0.12$; Fig. 5b) and modestly positive with the raw EOF ($r = 0.41$). Nevertheless, the corresponding PC timeseries is highly correlated with its raw-anomaly counterpart ($r = 0.89$) and very highly correlated with AIR ($r = 0.96$). It is also almost perfectly correlated with the all-India standardized anomaly average ($r = 0.99$) and the count of gridpoints with positive anomalies ($r = 0.97$). Note that the PCs computed from the raw vs. standardized anomaly EOFs need not be well correlated; that they are (and each even more so with AIR) further elucidates the complementary behaviors of the spatial extent of drying or wetting over India with the intensity of that drying or wetting over the high-variance regions.

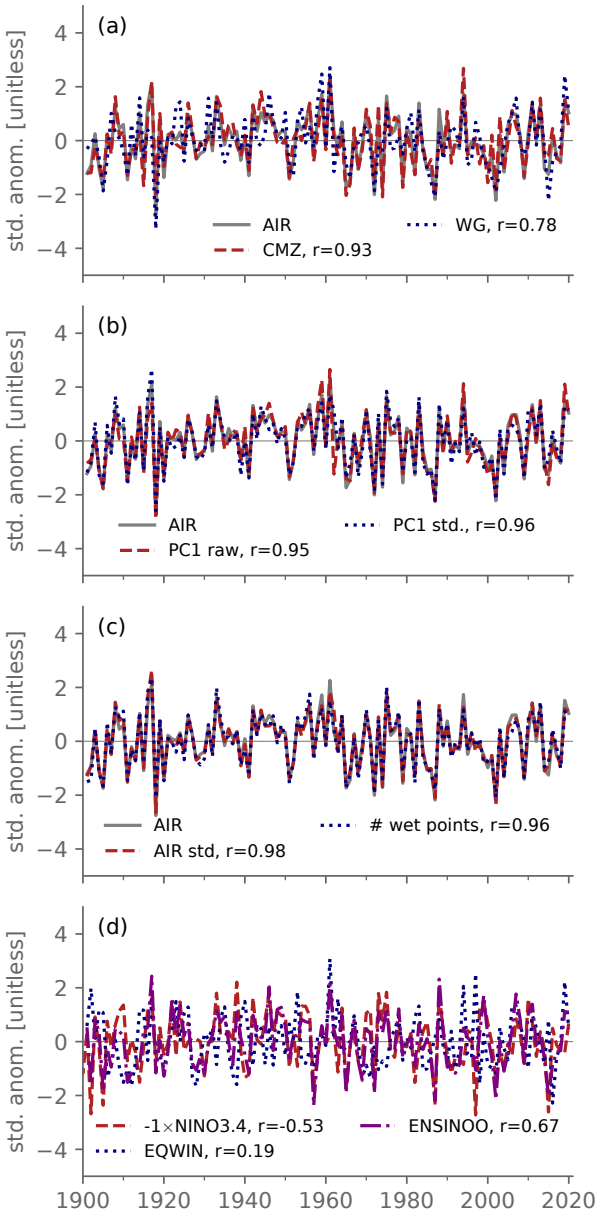

FIG. 4. Annual timeseries of JJAS-mean quantities, all as standardized anomalies (and thus unitless). In all panels, the solid gray is AIR, and other curves are as indicated in the panel's legend, along with their correlation coefficient with AIR. In (b), "AIR std." refers to the mean standardized anomaly over monsoonal India, rather than the mean raw anomaly as for AIR. In (c), "PC1 raw" and "PC1 std" refer to the first principal component timeseries computed from raw and standardized JJAS anomalies, respectively. In (d), "ENSINOO" refers to the combined ENSO-EQUINOO index computed as $-1\times$NINO3.4+0.64$\times$EQWIN.

c. Extreme dry and wet years

We have computed composites over the eight driest (1918, 2002, 1987, 1972, 1905, 1965, 1974, 1979) and, separately, eight wettest (1961, 1917, 1994, 1959, 1975, 1933, 2019, 1983) years in terms of the detrended JJAS AIR anomaly. The rainfall anomalies of these dry and wet composites are shown in Fig. 7(a) and Fig. 8(a), respectively. The spatial structures of the two composites are very similar (pattern correlation $r = -0.72$), with single-signed anomalies at the vast majority of gridpoints, the largest magnitudes in WG, followed by in CMZ, and smallest values, some taking the opposite sign, in the far east and peninsular India east of WG. The difference between them (map not shown, but included in pattern correlation matrix of Fig. 5b) resembles the rainfall mean and standard deviation fields ($r = 0.74$ and 0.76) and very closely resembles the first EOF just described ($r = 0.95$).

If a spatially homogeneous drying or wetting mode were the only operative one, it wouldn't be the case that AIR is so well correlated with the number of anomalously wet gridpoints—instead, in each year nearly all gridpoints would have the same sign, and the magnitude of those same-signed anomalies would increase or decrease. This can also be inferred from the point-to-point correlations described above (Fig. 3), with highly structured, alternating positive and negative correlations rather than simple decay toward zero moving away from the given point. This can also be seen from the individual dry and wet extreme years included in Fig. 7 and Fig. 8. In the wettest year (1961) anomalies are very positive over much of WG and the CMZ but are modestly negative over a considerable portion of peninsular India and various other clusters of points. Whereas in the second wettest year (1917) values are more homogeneous overall, although with dry anomalies in roughly half of WG. In contrast, the driest year (1918) anomalies are most negative within WG but also over nearly all other points, save for a few patches in the eastern CMZ.

Printed in the bottom-left of each panel are the pattern correlation coefficients between the raw rainfall anomalies shown in that panel with the first EOF from the raw anomalies (Fig. 6a) and between the standardized rainfall anomalies (not shown) with the first EOF from the standardized anomalies (Fig. 6b). For both dry and wet composites and a majority of the extreme 16 years shown, the pattern correlation with the EOFs is larger in magnitude when both are in terms of raw rainfall rather than standardized anomalies. At the same time, three of the eight wettest years (1917, 1975, and 1983, which are the 2nd, 5th, and 8th wettest years respectively) and the seventh driest year (1974) have higher magnitude pattern correlations in terms of standardized anomalies.

This suggests that, in addition to a mode of quasi-homogeneous drying or wetting, one or more additional mechanisms brings JJAS-mean rainfall anomalies more heterogeneously over India. We therefore now investigate the remote teleconnections that plausibly force these different behaviors.

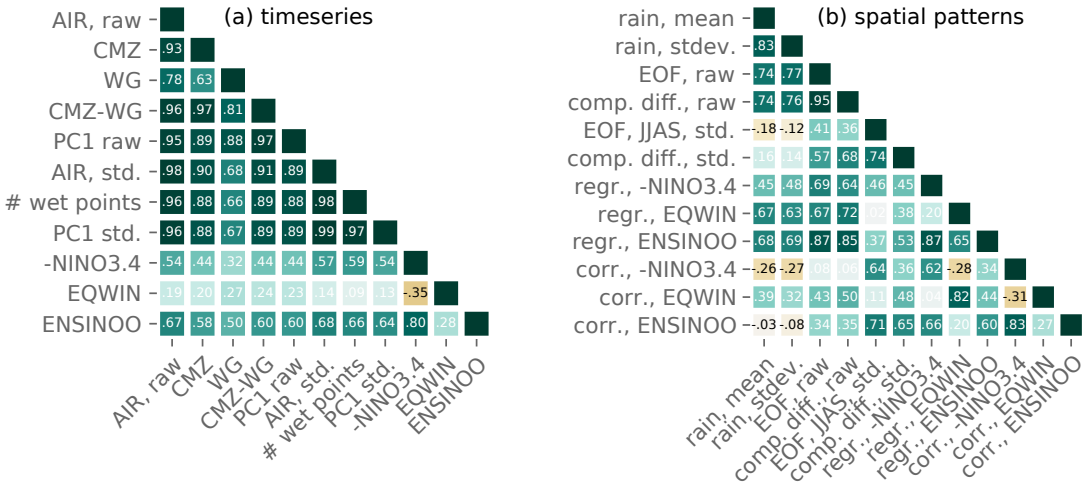

FIG. 5. Cross-correlation matrices showing the correlation coefficients (unitless) among (a) 120-year, detrended timeseries of JJAS-averaged quantities and (b) spatial patterns of quantities defined on a gridded basis over monsoonal India. In (a), quantities from top to bottom and left to right are: AIR average; CMZ region average; WG region average; the linear combination of CMZ and WG; the principal component corresponding to the first EOF computed from raw rainfall anomalies; the all-India average of standardized rainfall anomalies; the number of gridpoints in which the JJAS rainfall anomaly is positive; the principal component corresponding to the first EOF computed from standardized rainfall anomalies; the negative of the NINO3.4 index; the EQWIN index; and the combined NINO3.4-EQWIN index ENSINOO. In (b), quantities are: climatological JJAS rainfall; JJAS rainfall standard deviation; the first EOF computed from raw rainfall anomalies; the difference in raw rainfall anomalies between the extreme dry and wet year composites; the first EOF computed from standardized rainfall anomalies; the difference in standardized rainfall anomalies between the extreme dry and wet year composites; the rainfall regression on $-1\times$NINO3.4; the rainfall regression on EQWIN; the rainfall regression on ENSINOO; the rainfall correlation with $-1\times$NINO3.4; the rainfall correlation with EQWIN; and the rainfall correlation with ENSINOO.

4. Teleconnections

The JJAS timeseries of -1×NINO3.4 and EQWIN are shown in Fig. 4(d) and included in the correlation matrix in Fig. 5(a), the sign of NINO3.4 flipped so that positive values correspond to positive AIR anomalies (as they do for EQWIN). NINO3.4 and EQWIN are modestly correlated with one another ($r = 0.34$); note this differs appreciably from Surendran et al. (2015) who found $r = 0.01$ using different and shorter duration datasets.

Following Surendran et al. (2015), we create a combined ENSO-EQUINOO timeseries, "ENSINOO," (also shown in the same figure panels) with relative weights of -1 for NINO3.4 and +0.64 for EQWIN chosen to optimize the correlation with AIR over the 1901-2020 time period. The ENSINOO timeseries (Fig. 4d) is well correlated with AIR ($r = 0.67$; Fig. 5(a)), more so (by construction) than are either $-1\times$NINO3.4 or EQWIN ($r = 0.54$ and 0.19, respectively). EQWIN's positive correlation with AIR comes despite EQWIN being positively (albeit modestly) correlated with NINO3.4, since El Niño otherwise tends to dry India.

Fig. 9 shows maps of the JJAS rainfall anomaly regression at each gridpoint on each of $-1\times$NINO3.4, EQWIN, and ENSINOO. For -1×NINO3.4, the regression is positive at most gridpoints of monsoonal India, consistent with the prevailing wisdom that El Niño has a pervasive drying influence over the whole subcontinent (e.g. Ashok et al. 2019). Regressions are most positive in the WG directly along the coast, least positive (including some slightly negative values) in the far east of the CMZ, and relatively homogeneous elsewhere. This homogeneity results from compensating factors: large variance but modest correlations in the CMZ vs. small variance but larger correlations in non-WG peninsular India. A local minimum in the correlation runs along the axis of the Western Ghats mountain range, which explains the modest regression there compared to the coastal points just to the west.

For EQWIN, compared to NINO3.4 there is more regional structure. Positive values span the WG and most of the CMZ, while negative values span much of the Deccan plateau and north of the CMZ. The spatial pattern resembles those of the climatological rainfall mean ($r = 0.67$), standard deviation ($r = 0.63$), the pointwise correlations with points in the WG (Fig. 3b), and the first EOF computed from raw rainfall anomalies ($r = 0.67$).

The combined index ENSINOO being weighted more strongly to $-1\times$NINO3.4 than to EQWIN, its regression more closely resembles that of NINO3.4 (pattern correlation $r = 0.87$; Fig. 5b) than that of EQWIN ($r = 0.65$). The fingerprints of EQWIN are more positive loadings in WG, reduced (but still positive) loadings to the east thereof, and more positive loadings over much of the CMZ, including

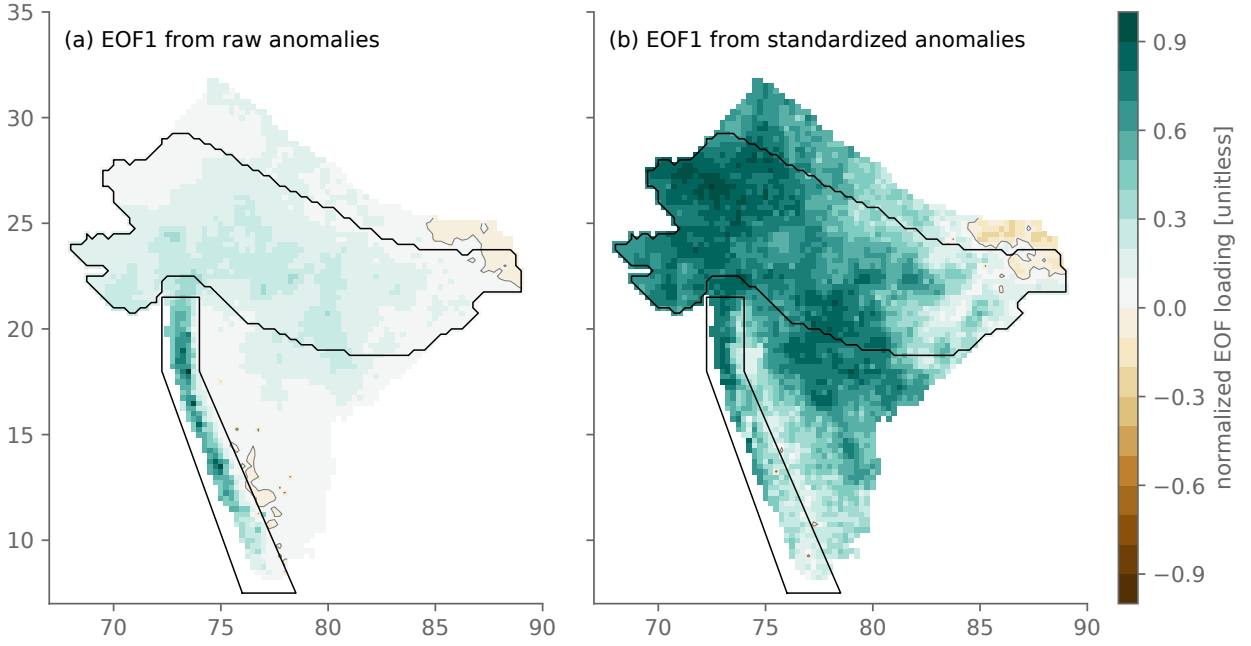

FIG. 6. First EOF of JJAS-mean rainfall computed either from (left column) raw anomalies or (right column) standardized anomalies at each gridpoint. In each panel, values are normalized by that EOF's maximal value, and solid gray contours signify that EOF's zero contour.

in the far east such that the expanse of negative values there contracts appreciably. Combined, these yield an ENSINOO teleconnection that is almost entirely same-signed and whose rainfall regression pattern closely resembles the first EOF of raw seasonal rainfall anomalies ($r = 0.87$).

Printed in each panel of Fig. 7 and Fig. 8 are the NINO3.4 and EQWIN values for that year (or for the composite, the average over the years being composited). In the single wettest year, 1961, NINO3.4 was very small, -0.2, but EQWIN was very large, 3.1. In the second wettest year, 1917, a clear La Niña event occurred with NINO3.4 at -1.6, promoting wetting along with EQWIN at 1.5. In the third wettest year, 1994, NINO3.4 was actually positive, 0.9, but this was partially countered by a strongly positive EQWIN, 2.1. And in the fourth wettest year, 1959, the excess rainfall evidently was driven by other processes, as both NINO3.4 and EQWIN values were modest (-0.5 and 0.2).

ENSO operates on an interannual timescale and as such varies little over the course of any individual JJAS, let alone on subseasonal timescales (not shown). For that reason, it can be very credibly interpreted as a remote forcing that causes changes in Indian summer monsoon rainfall. To the extent that EQUINOO primarily reflects the forcing by the underlying SST anomalies associated with the IOD, which operates on comparable timescales (though with greater seasonal phase-locking than ENSO), it too can be considered a remote teleconnection. But this is not entirely the case, as can be seen from Fig. 10, showing the daily value of EQWIN computed from ERA5 over JJAS of 1990 along with its seasonal-mean value for that year; other years not shown yield similar inferences. Daily variability greatly exceeds interannual variability in the seasonal-mean (compare to Fig. 4), and it is plausible that intraseasonal mechanisms such as the Madden-Julian Oscillation would imprint on the near-surface wind in the central equatorial Indian Ocean that defines the EQWIN index, as they do on Indian summer monsoon rainfall (Pai et al. 2011), calling the direction of causality of the EQUINOO teleconnection into question.

5. Results in the pre-satellite vs. satellite eras

Motivated by past literature documenting changes in time of the teleconnection strength of ENSO on Indian summer monsoon rainfall, we repeat our teleconnection and EOF calculations separately over the pre-satellite era of 1901-1979 and the satellite era of 1979-2020. The results are insensitive to whether trends are removed over the full 1901-2020 period, over each specific period, or not at all (not shown); as such all results plotted and quoted are for the 1901-2020 detrended timeseries. In the pre-satellite era, JJAS AIR is highly correlated with $-1\times$NINO3.4, $r = 0.60$, and weakly with EQWIN, $r = 0.06$. Going to the satellite era, the correlation magnitude decreases appreciably for $-1\times$NINO3.4, to $r = 0.41$, and increases even more for EQWIN, to $r = 0.41$. Taken

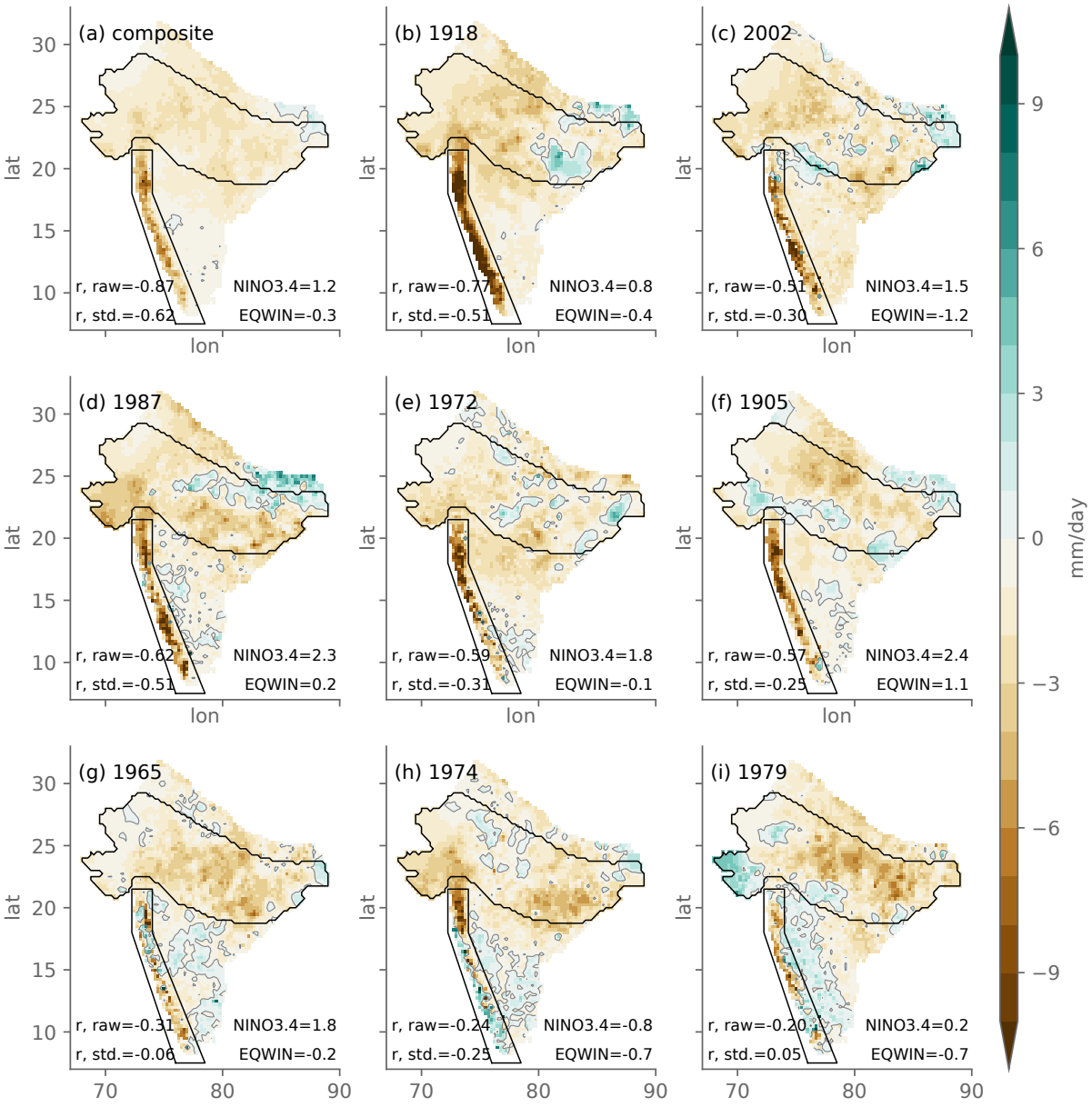

FIG. 7. JJAS rainfall anomalies, in mm day^{-1}, (a) composited over the eight driest years in terms of the JJAS all-monsoonal India average, and (b-i) for each of those eight individual years, in rank order, with the year printed. Also printed in each panel are the JJAS-averaged NINO3.4 and EQWIN index values for that year (or for the composite, averaged over all eight years) and the pattern correlations between the given anomaly pattern and the first EOF computed from either raw or standardized JJAS-mean rainfall anomalies.

at face value, this suggests, surprisingly, that in the modern climate AIR is more closely related to EQUINOO than it is to ENSO.

By comparison, the correlation between NINO3.4 and EQWIN is fairly stable, $r = 0.37$ and $r = 0.33$ in the pre-satellite and satellite eras, respectively. This, combined with the opposite-signed changes in for $-1\times$NINO3.4 vs. EQWIN in the correlation with AIR, results in the combined index ENSINOO having a much more stable correlation with AIR, varying only from $r = 0.66$ to $r = 0.69$ from the pre-satellite to satellite eras.

Fig. 11 shows the rainfall regression maps for each of $-1\times$NINO3.4, EQWIN, and ENSINOO in the pre-satellite era, the satellite era, and the difference between the eras. For $-1\times$NINO3.4, regressions are positive at the vast majority of gridpoints for both the full duration (1901-

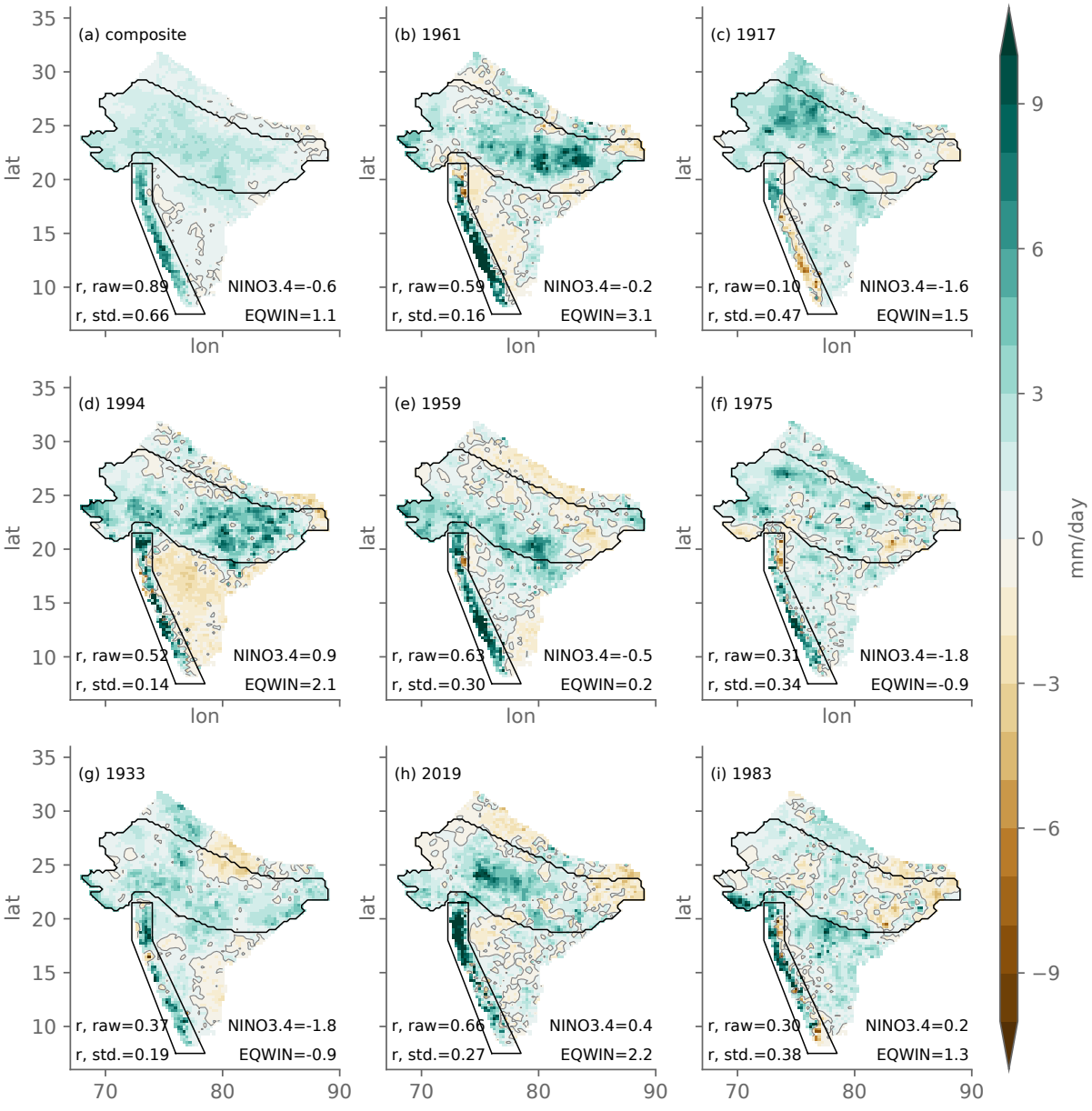

FIG. 8. Same as Fig. 7, but for the eight wettest rather than driest years.

2020; c.f. Fig. 9a) and the pre-satellite era, but during the satellite era (1979-2020) values over much of the CMZ decrease appreciably, either becoming less positive or negative. The same holds though to a lesser extent within WG. For EQWIN, values become more positive over most of monsoonal India in the satellite vs. pre-satellite era, especially in the WG and in the western CMZ, such that the expanse of negative values from southeast India extending northwest contracts. For ENSINOO, these changes in the NINO3.4 and EQWIN regressions generate considerable cancellation, such that the regression pattern is more stable between the two eras than for either teleconnection mode alone. That said, the ENSINOO regression becomes less positive over most of the CMZ, except for the far west, and becomes more positive over much of WG and southeast India.

We do not have a compelling explanation for this seeming compensation between the changing nature of the ENSO vs. EQUINOO teleconnections. These multidecadal changes could reflect internal variability, a forced

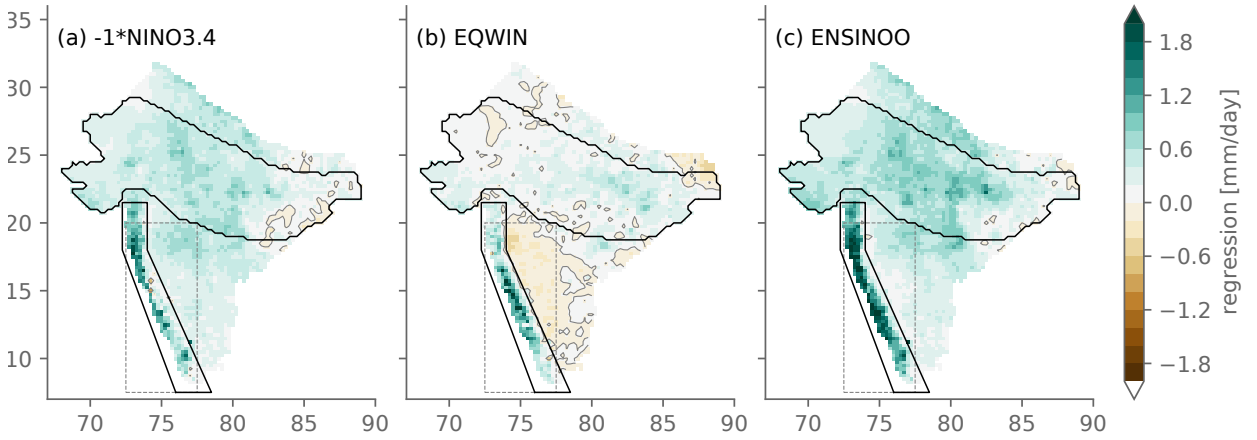

FIG. 9. Maps of JJAS local rainfall regression slope with (a) -1×NINO3.4, (b) EQWIN, and (c) the combined ENSINOO index defined as -1*NINO3.4 + 0.64*EQWIN. All indices are dimensionless quantities and the units are therefore mm day^{-1}. The zero contour is shown as a thin grey contour.

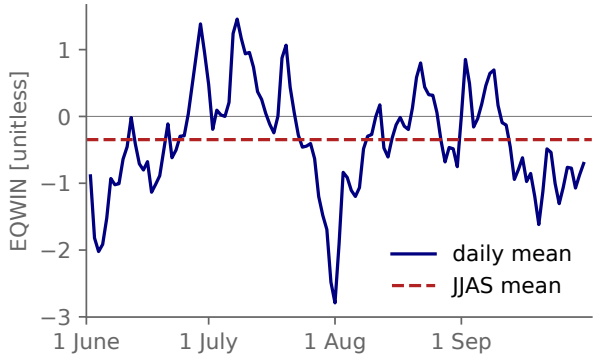

FIG. 10. In solid blue, daily timeseries of EQWIN over JJAS of 1990, along with its seasonal-mean value in dashed red.

response to anthropogenic forcing, or artifacts due to the changing observational network. Lin and Huybers (2019) show that trends in extreme rainfall using the same IMD rainfall 0.25×0.25° dataset are heavily influenced by changes in the station distribution. And Moron et al. (2017) argue that local daily rainfall distributions in India during summer are to good approximation exponential, such that the extremes strongly influence the mean. Also, 1979 is when the ERA5 dataset switches from the provisional, "extended" reanalysis that spans 1950-1978. If conversely these multi-decadal changes predominantly reflect forced responses to anthropogenic forcing, then the interpretation of the long-term average should be modified accordingly, and averages over the satellite era likely become more relevant in informing efforts to predict future summer monsoon interannual variability (at the expense of increased noise).

6. Conclusions

All-India rainfall (AIR) averaged over JJAS is a widely used indicator of the bulk Indian summer monsoon behavior that is physically intuitive and has demonstrated links to Indian agricultural and economic outcomes. By construction, the behavior of AIR will primarily reflect that of Indian sub-regions with largest variance, namely the CMZ and WG, calling into question its relevance for other regions of India in which the mean and variance of JJAS rainfall are lower. But past studies have argued that the predominant variability mode influencing AIR is a quasi-homogeneous drying or wetting signal encompassing both the low- and high- rainfall regions, which others in turn associate with ENSO. But the correlation of AIR with ENSO has weakened since the early 20th century, while the correlation of AIR with the quasi-uniform mode (deduced from empirical orthogonal function analysis) has persisted. Another teleconnection mode, EQUINOO, has been introduced in recent decades, but its behavior in the early 20th century has not been investigated, and even for the more modern period the details of its spatial imprint on Indian rainfall and its temporal characteristics remain imperfectly understood. We revisit these issues using modern, long-duration SST, reanalysis, and high-resolution gridded rainfall datasets.

We find that AIR is almost perfectly correlated both with the raw rainfall anomalies averaged over only the CMZ and WG sub-regions and with standardized rainfall anomalies averaged over the entire subcontinent. In other words, despite rainfall variance being concentrated in the CMZ and WG, there is evidently a quasi-homogeneous signal on the seasonal timescale that acts on both these high-variance regions and most of the rest of monsoonal India. Years in which CMZ and WG are very wet (or dry)

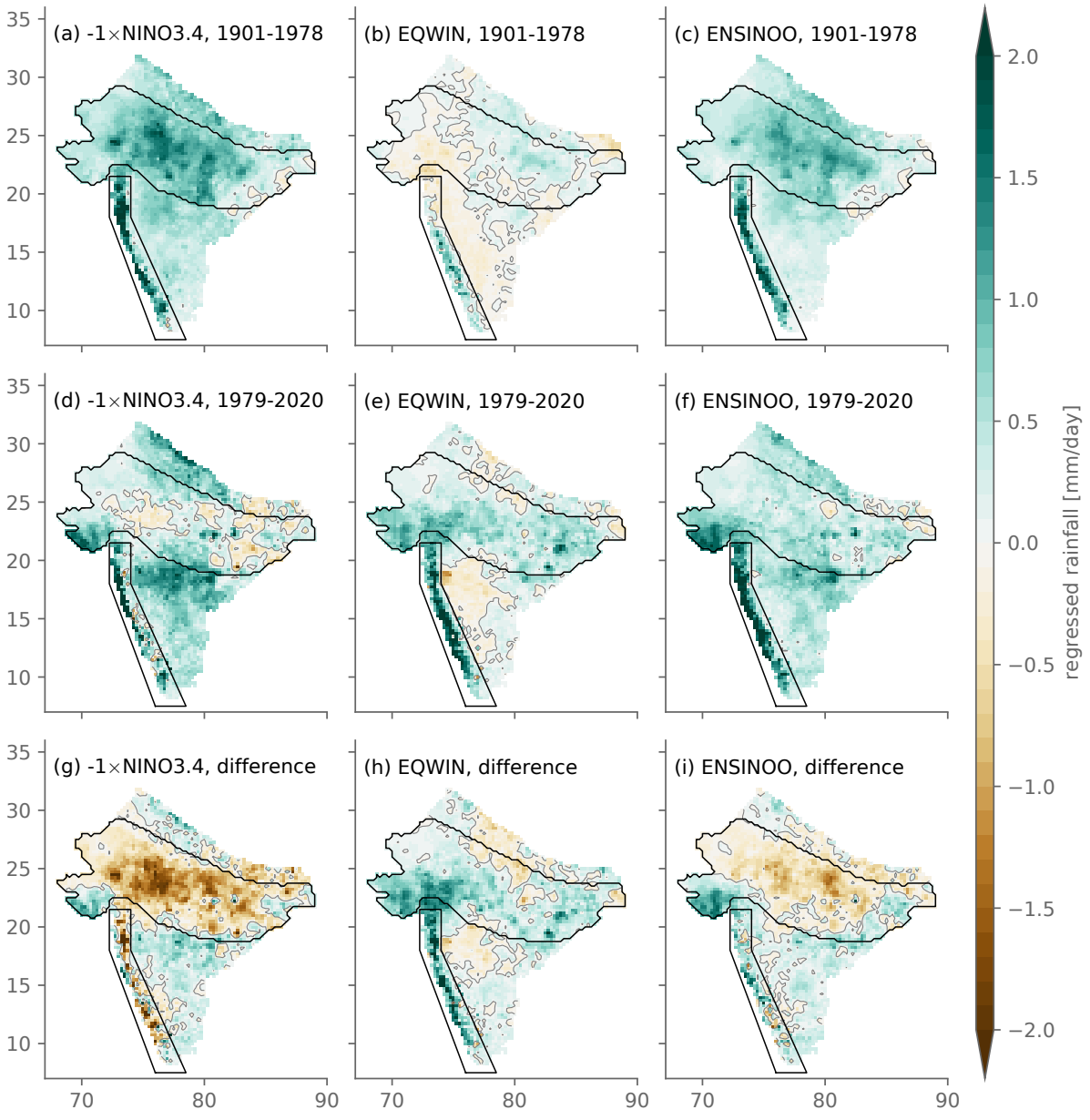

FIG. 11. Regression of JJAS rainfall on the three teleconnection indices, (columns, left to right) -1*NINO3.4, EQWIN, and the combined NINO3.4-EQWIN index ENSINOO, computed over (top row) the pre-satellite era of 1901-1978, (middle row) the satellite era of 1979-2020, or (bottom row) the satellite era minus the pre-satellite era. All indices are dimensionless quantities and the units are therefore mm day^{-1}. The zero contour is shown as a thin grey contour. The results can be compared to corresponding fields for the full 1901-2020 period in Fig. 9.

also tend to be years where the rest of India is, relative to local deviations, very wet (or dry).

We confirm the well-known overall drying tendency of El Niño on the Indian summer monsoon but also the decrease in strength of that relationship going from the pre-satellite to satellite eras. We show for the first time that, for reasons not yet understood, the relationship between Indian JJAS rainfall and EQUINOO changes in a largely compensating manner over the same epochs. As such, a combined ENSO-EQUINOO index we introduce (c.f. Surendran et al. 2015), ENSINOO, is comparatively stable over the full 120-year period. And because ENSO and EQUINOO are only moderately correlated with each other, its correlation with AIR is appreciably higher than that of either teleconnection mode alone with AIR.

However, EQUINOO, like AIR but unlike ENSO, exhibits greater variance on daily than on seasonal timescales. This, along with EQUINOO's weak correlation on the seasonal-mean timescale with the IOD, raises questions about how much the EQUINOO influence on Indian summer monsoon rainfall should be considered a remotely forced signal—and therefore in principle predictable months or more in advance. In other words, it remains to be determined how much the stability of ENSINOO is the result of a jointly operating teleconnection mode previously unidentified or merely the counterbalancing changes between the remote ENSO signal strength vs. the seasonal residual of unforced, large-magnitude subseasonal variations counterbalancing change.

That the CMZ and WG region-mean JJAS rainfall anomalies are well correlated ($r = 0.59$) differs from the results of Vecchi and Harrison (2004) who find two similar-but-different regions weakly correlated ($r \approx 0.2$). This is due to that study's WG region spanning into peninsular India (borders overlain in Fig. 3), including points for which rainfall anomalies are anti-correlated with those along the coast. Using the Vecchi and Harrison (2004) region definitions applied to the IMD $0.25^\circ \times 0.25^\circ$ dataset 1901-2020 we use, the cross-region correlation is low (not shown). The $2.5^\circ \times 2.5^\circ$ CMAP dataset available at the time is too coarse to resolve the narrow, $\sim 1^\circ$ longitude wide rainfall regime from the coast to the mountains, nor the sharp gradient between there and the rain-shadow just beyond.

From the perspective of agricultural yields integrated over the country, it is perhaps more useful to think of AIR in terms of how it manifests in standardized anomalies: local vegetation presumably is adapted to its local hydroclimate and rainfall variability. In other words, a 10 mm/day anomaly will matter more in a location where the standard deviation is 5 mm/day than 20 mm/day. But perhaps for other societal applications such as flooding and for the atmospheric circulation through latent heating, it is plausible that the raw rainfall anomalies, irrespective of their climatological value or typical variations, matter more. It would be interesting to revisit the analyses of Gadgil and Gadgil (2006) on the relationships among monsoon rainfall, Indian agricultural yields, and Indian gross domestic product, but using these alternative measures that more closely reflect the spatial extent of wet or dry anomalies rather than their average.

Acknowledgments. All authors acknowledge support from the Monsoon Mission Project under India's Ministry of Earth Sciences. S.A.H. acknowledges funding from the Columbia University Earth Institute Postdoctoral Fellowship. We thank Sulochana Gadgil for many valuable discussions and comments. We thank P. Mukhopadhyay and P. Pillai for helpful comments.

IMD rainfall data used is available at `https://www.imdpune.gov.in/Clim_Pred_LRF_New/Grided_Data_Download.html`. ERA5 data is available at `https://cds.climate.copernicus.eu/#!/search?text=ERA5&type=dataset`. NOAA OI SST data is available at `https://psl.noaa.gov/data/gridded/data.noaa.oisst.v2.html`. ERSST data is available at `https://www.ncei.noaa.gov/pub/data/cmb/ersst/v5/netcdf/`

References

Ashok, K., F. Feba, and C. T. Tejavath, 2019: The Indian summer monsoon rainfall and ENSO. *Mausam*, **70 (10)**, 443–452.

Blanford, H. F., 1886: *The Rainfall of India*. India Meteorological Department, Calcutta.

Charney, J. G., and J. Shukla, 1981: Predictability of Monsoons. *Monsoon Dynamics*, 1st ed., Cambridge University Press, doi:10.1017/CBO9780511897580.

Francis, P. A., and S. Gadgil, 2006: Intense rainfall events over the west coast of India. *Meteorol. Atmos. Phys.*, **94 (1)**, 27–42, doi:10.1007/s00703-005-0167-2.

Francis, P. A., and S. Gadgil, 2013: A note on new indices for the equatorial Indian Ocean oscillation. *J Earth Syst Sci*, **122 (4)**, 1005–1011, doi:10.1007/s12040-013-0320-0.

Gadgil, S., 2003: The Indian Monsoon and Its Variability. *Annual Review of Earth and Planetary Sciences*, **31 (1)**, 429–467, doi:10.1146/annurev.earth.31.100901.141251.

Gadgil, S., 2018: The monsoon system: Land–sea breeze or the ITCZ? *J Earth Syst Sci*, **127 (1)**, 1, doi:10.1007/s12040-017-0916-x.

Gadgil, S., and S. Gadgil, 2006: The Indian Monsoon, GDP and Agriculture. *Economic and Political Weekly*, **41 (47)**, 4887–4895.

Gadgil, S., K. Rajendran, and D. S. Pai, 2019: A new rain-based index for the Indian summer monsoon rainfall. *Mausam*, **70 (3)**, 485–500.

Gadgil, S., P. N. Vinayachandran, and P. A. Francis, 2003: Droughts of the Indian summer monsoon: Role of clouds over the Indian Ocean. *Current Science*, **85 (12)**, 1713–1719.

Gadgil, S., P. N. Vinayachandran, P. A. Francis, and S. Gadgil, 2004: Extremes of the Indian summer monsoon rainfall, ENSO and equatorial Indian Ocean oscillation. *Geophysical Research Letters*, **31 (12)**, L12 213, doi:10.1029/2004GL019733.

Gadgil, S., Yadumani, and N. V. Joshi, 1993: Coherent rainfall zones of the Indian region. *International Journal of Climatology*, **13 (5)**, 547–566, doi:10.1002/joc.3370130506.

Hersbach, H., and Coauthors, 2020: The ERA5 Global Reanalysis. *Quarterly Journal of the Royal Meteorological Society*, **n/a (n/a)**, doi:10.1002/qj.3803.

Huang, B., and Coauthors, 2015: Extended Reconstructed Sea Surface Temperature Version 4 (ERSST.v4). Part I: Upgrades and Intercomparisons. *J. Climate*, **28 (3)**, 911–930, doi:10.1175/JCLI-D-14-00006.1.

Huffman, G. J., and Coauthors, 2007: The TRMM Multisatellite Precipitation Analysis (TMPA): Quasi-Global, Multiyear, Combined-Sensor Precipitation Estimates at Fine Scales. *J. Hydrometeor*, **8 (1)**, 38–55, doi:10.1175/JHM560.1.

Hunt, K. M. R., A. G. Turner, T. H. M. Stein, J. K. Fletcher, and R. K. H. Schiemann, 2021: Modes of coastal precipitation over southwest India and their relationship with intraseasonal variability. *Quarterly Journal of the Royal Meteorological Society*, **147 (734)**, 181–201, doi:10.1002/qj.3913.

Kelkar, R. R., and O. P. Sreejith, 2020: Meteorological sub-divisions of India and their geopolitical evolution from 1875 to 2020. *Mausam*, **71 (4)**, 571–584.

Krishnamurthy, V., and R. S. Ajayamohan, 2010: Composite Structure of Monsoon Low Pressure Systems and Its Relation to Indian Rainfall. *J. Climate*, **23 (16)**, 4285–4305, doi:10.1175/2010JCLI2953.1.

Krishnamurthy, V., and J. Shukla, 2000: Intraseasonal and Interannual Variability of Rainfall over India. *J. Climate*, **13 (24)**, 4366–4377, doi:10.1175/1520-0442(2000)013⟨0001:IAIVOR⟩2.0.CO;2.

Krishnamurthy, V., and J. Shukla, 2007: Intraseasonal and Seasonally Persisting Patterns of Indian Monsoon Rainfall. *J. Climate*, **20 (1)**, 3–20, doi:10.1175/JCLI3981.1.

Krishnamurthy, V., and J. Shukla, 2008: Seasonal persistence and propagation of intraseasonal patterns over the Indian monsoon region. *Clim Dyn*, **30 (4)**, 353–369, doi:10.1007/s00382-007-0300-7.

Laloyaux, P., and Coauthors, 2018: CERA-20C: A Coupled Reanalysis of the Twentieth Century. *Journal of Advances in Modeling Earth Systems*, **10 (5)**, 1172–1195, doi:10.1029/2018MS001273.

Lin, M., and P. Huybers, 2019: If Rain Falls in India and No One Reports It, Are Historical Trends in Monsoon Extremes Biased? *Geophysical Research Letters*, **46 (3)**, 1681–1689, doi:10.1029/2018GL079709.

Moron, V., A. W. Robertson, and D. S. Pai, 2017: On the spatial coherence of sub-seasonal to seasonal Indian rainfall anomalies. *Clim Dyn*, **49 (9)**, 3403–3423, doi:10.1007/s00382-017-3520-5.

Nie, J., W. R. Boos, and Z. Kuang, 2010: Observational Evaluation of a Convective Quasi-Equilibrium View of Monsoons. *Journal of Climate*, **23 (16)**, 4416–4428, doi:10.1175/2010JCLI3505.1.

Pai, D. S., J. Bhate, O. P. Sreejith, and H. R. Hatwar, 2011: Impact of MJO on the intraseasonal variation of summer monsoon rainfall over India. *Clim Dyn*, **36 (1-2)**, 41–55, doi:10.1007/s00382-009-0634-4.

Pai, D. S., L. Sridhar, M. Rajeevan, O. P. Sreejith, N. S. Satbhai, and B. Mukhopadhyay, 2014: Development of a new high spatial resolution (0.25° × 0.25°) long period (1901-2010) daily gridded rainfall data set over India and its comparison with existing data sets over the region. *Mausam*, **65 (1)**, 18.

Palmer, T. N., 1994: Chaos and predictability in forecasting the monsoons. *Proc. Indian Natl. Sci. Acd.*, **60**, 57–66.

Rajeevan, M., S. Gadgil, and J. Bhate, 2010: Active and break spells of the Indian summer monsoon. *J Earth Syst Sci*, **119 (3)**, 229–247, doi:10.1007/s12040-010-0019-4.

Rasmusson, E. M., and T. H. Carpenter, 1983: The Relationship Between Eastern Equatorial Pacific Sea Surface Temperatures and Rainfall over India and Sri Lanka. *Mon. Wea. Rev.*, **111 (3)**, 517–528, doi:10.1175/1520-0493(1983)111⟨0517:TRBEEP⟩2.0.CO;2.

Reynolds, R. W., N. A. Rayner, T. M. Smith, D. C. Stokes, and W. Wang, 2002: An Improved In Situ and Satellite SST Analysis for Climate. *J. Climate*, **15 (13)**, 1609–1625, doi:10.1175/1520-0442(2002)015⟨1609:AIISAS⟩2.0.CO;2.

Saji, N. H., B. N. Goswami, P. N. Vinayachandran, and T. Yamagata, 1999: A dipole mode in the tropical Indian Ocean. *Nature*, **401 (6751)**, 360–363, doi:10.1038/43854.

Sikka, D. R., and S. Gadgil, 1980: On the Maximum Cloud Zone and the ITCZ over Indian Longitudes during the Southwest Monsoon. *Mon. Wea. Rev.*, **108 (11)**, 1840–1853, doi:10.1175/1520-0493(1980)108⟨1840:OTMCZA⟩2.0.CO;2.

Surendran, S., S. Gadgil, P. A. Francis, and M. Rajeevan, 2015: Prediction of Indian rainfall during the summer monsoon season on the basis of links with equatorial Pacific and Indian Ocean climate indices. *Environ. Res. Lett.*, **10 (9)**, 094 004, doi:10.1088/1748-9326/10/9/094004.

Vecchi, G. A., and D. E. Harrison, 2004: Interannual Indian Rainfall Variability and Indian Ocean Sea Surface Temperature Anomalies. *Earth's Climate: The Ocean-Atmosphere Interaction*, No. 147, Geophysical Monographs, American Geophysical Union (AGU), 247–259, doi:10.1029/147GM14.

Webster, P. J., A. M. Moore, J. P. Loschnigg, and R. R. Leben, 1999: Coupled ocean–atmosphere dynamics in the Indian Ocean during 1997–98. *Nature*, **401 (6751)**, 356–360, doi:10.1038/43848.